JOURNAL OF OCULAR PHARMACOLOGY AND THERAPEUTICS
Volume 00, Number 00, 2013

DOI: 10.1089/jop.2013.0182

SPECIAL ISSUE

Multi-Scale Analysis of Segmental Outflow Patterns in Human Trabecular Meshwork with Changing Intraocular Pressure

Jason Y.H. Chang,[1,*] Steven J. Folz,[2,*] Susuana N. Laryea,[1] and Darryl R. Overby[1,2]

Abstract

Purpose: Aqueous humor filtration in the trabecular meshwork is believed to be non-uniform or ''segmental'' such that only a fraction of trabecular meshwork is filtration-active at any given instant. The goal was to quantify the filtration-active fraction of human trabecular meshwork and to determine how filtration patterns change with outflow facility and intraocular pressure (IOP).
Methods: Six pair of enucleated human eyes were perfused with fluorescent tracer microspheres (0.2 μm) at 7 or 30 mmHg. Tracer patterns were imaged over the ''macro-scale'' (0.1–10 mm) using epifluorescence microscopy and ''micro-scale'' (10–100 μm) using confocal microscopy. Quantitative image analysis was used to measure the tracer-labeled fraction and to examine co-localization with trabecular pigmentation and the location of collector channel ostia.
Results: Tracer distribution was segmental over both macro-scale and micro-scale dimensions. No more than approximately one-third of the trabecular meshwork appeared to be filtration-active on the macro scale ($29\% \pm 5\%$; mean ± SD) and micro scale ($21\% \pm 6\%$). There was weak co-localization between macro-scale tracer intensity and pigmentation ($r = 0.17$, $P = 0.017$), and collector channel ostia tended to coincide with regions of high macro-scale tracer intensity. Tracer patterns were relatively insensitive to changing IOP over hour-long time scales and did not correlate with outflow facility.
Conclusions: Filtration patterns in human trabecular meshwork appear segmental over both macro-scale and micro-scale dimensions, with only approximately one-third of the trabecular meshwork actively contributing to outflow. Segmental outflow may limit the efficacy of outflow drugs by preventing delivery to non-filtering trabecular regions that may contribute the most to outflow obstruction in glaucoma.

Introduction

THE BULK OF aqueous humor outflow resistance is likely generated near the inner wall endothelium of Schlemm's canal and the subjacent juxtacanalicular connective tissue (JCT)[1–4], but the hydrodynamic details of how aqueous humor flows through these tissues and how these tissues generate outflow resistance are not well understood. Tracer studies[5–9] and studies of pigment distribution in the trabecular meshwork[10–12] have suggested that aqueous humor outflow is ''segmental'' rather than uniform, such that only a fraction of the total area of JCT and inner wall is involved in aqueous humor filtration at any given instant. Since segmental outflow influences the filtration function of the trabecular meshwork and may control the delivery of molecular therapeutics that are aimed at enhancing outflow, it is important to understand what fraction of the trabecular meshwork actively contributes to filtration and how filtration patterns change in response to physiologic parameters such as intraocular pressure (IOP) and outflow facility.

Previous works in bovine eyes has shown that filtration patterns within the trabecular meshwork are sensitive to IOP[7,13,14] and that the apparent fraction of JCT and inner wall involved in filtration correlates with outflow facility.[8,13,15–17] Therefore, it would appear that trabecular filtration patterns and the morphologic factors controlling these patterns are important determinants of outflow resistance generation. Consistent with this idea is the finding that the trabecular filtration area appears to be further reduced in glaucomatous eyes,[5] suggesting that segmental outflow may further limit the delivery of anti-glaucoma drugs to underperfused regions of the trabecular meshwork.

[1]Department of Bioengineering, Imperial College London, London, United Kingdom.
[2]Department of Biomedical Engineering, Tulane University, New Orleans, Louisiana.
*These authors are co-first authors.

In this article, we investigate filtration patterns in the trabecular meshwork of enucleated human eyes after perfusion with fluorescent tracer microspheres. Our goals are to quantify the fraction of trabecular meshwork that appears to be filtration-active and to determine whether filtration patterns are sensitive to IOP and correlate with outflow facility. We examine filtration patterns over 2 length scales: the ''*macro*-scale'' where tracer patterns are visualized at 10× magnification over the entire circumference of trabecular meshwork *en face* (scale of 0.1–10 mm); and the ''*micro*-scale'' where tracer patterns are visualized at 200× magnification over cellular-level dimensions (10–100 μm) near the inner wall using confocal microscopy.

Methods

Fluorescent tracer microspheres

Our experimental design uses a 2-color fluorescent tracer perfusion to label filtration patterns in the human trabecular meshwork.[13,14] One tracer color is perfused at baseline pressure (7 or 30 mmHg) followed by perfusion with a different tracer color after changing IOP. This approach is advantageous, because it enables a direct comparison of pre- and post-stimulus tracer patterns within individual sections, considerably increasing statistical sensitivity to detect subtle pattern changes because each section has its own internal control. Fluorescent tracer microspheres (0.2 μm diameter FluoSpheres®; Invitrogen) were perfused at a concentration of 0.002% by volume (5×10^9 particles/mL) in perfusion medium. The perfusion fluid was Dulbecco's phosphate-buffered saline with 5.5 mM glucose (referred to as ''DBG'') that was passed through a 0.22 μm filter before use. The microspheres had a carboxylate coating, yielding a negative net surface charge at neutral pH. For the 2-color technique, each eye was perfused first with yellow-green (505 nm/515 nm) and subsequently, with red microspheres (580 nm/605 nm). All tracer-containing solutions were sonicated to break up aggregates before perfusion.

Perfusion and outflow facility measurements

Six pairs of ostensibly normal human eyes were obtained from the National Disease Research Interchange (NDRI) and delivered chilled to our Tulane laboratory overnight. The mean donor age was 63 years (range 36–80), and the mean postmortem time was 37.7 h (range 32.6–40.7). Other than 2 pairs being pseudophakic, all eyes were ostensibly free of ocular disease. All perfusions were performed intracamerally with whole globes at 34°C using a pressure-controlled computerized perfusion system[18] that was set to 7 or 30 mmHg (corresponding to 15 or 38 mmHg *in vivo*). Three of the 6 pairs were perfused at a baseline IOP of 7 mmHg that was increased partway through the perfusion to 30 mmHg in one eye of each pair, while the contralateral control eye was maintained at 7 mmHg. The other 3 pairs were treated with the opposite protocol, starting with a baseline IOP of 30 mmHg that was decreased to 7 mmHg in one eye.

Here, we describe the detailed perfusion protocol, a summary of which is given in Fig. 1. The sub-scripted symbols $C_0, C_1, C_2 \ldots$ refer to outflow facility measured during the corresponding period of the perfusion experiment. In the baseline period, each eye was perfused with DBG at baseline pressure (7 or 30 mmHg) to measure baseline facility (C_0). The duration of this period was varied to achieve approximately 30 min of stable facility data. The contents of the anterior chamber were then exchanged to deliver DBG containing the first (green) tracer. The volume exchanged through the anterior chamber was approximately 7 mL that was confirmed by fluorophotometry to be sufficient to completely deliver or remove tracer from the anterior chamber (Supplementary Fig. S1; Supplementary Data are available online at www.liebertpub.com/jop). After the exchange, the first tracer was perfused through the trabecular meshwork (C_1). The perfused volume during this period and all subsequent periods was fixed at approximately 100 μL, so as to deliver a known quantity of tracer to the trabecular meshwork and to control for any volume-dependent washout of tracer from the tissue. After the C_1 perfusion, the first tracer was removed by anterior chamber exchange with DBG alone, followed by perfusion with DBG at baseline pressure (C_2). In experimental eyes, IOP was then changed from 7 to 30 mmHg (or from 30 to 7 mmHg), followed by an additional perfusion period with DBG alone (C_3). In the contralateral control eyes, IOP was maintained at the baseline pressure throughout. The second (red) tracer was then exchanged into the anterior chamber and perfused (C_4). The second tracer was then removed by exchange, followed by perfusion with DBG alone (C_5). Finally, each eye was perfusion fixed at the prescribed pressure by exchange and perfusion (C_5) with 4% paraformaldehyde (PFA).

Tracer imaging

We examined tracer filtration patterns over 2 distinct length scales: (1) the *macro scale*, where we visualized tracer patterns over the entire circumference of trabecular meshwork viewed *en face* using epifluorescence microscopy at 10× magnification; and (2) the *micro scale*, where we visualized tracer patterns over cellular-level dimensions (200×) near the inner wall endothelium of Schlemm's canal and JCT using confocal microscopy.

For macro-scale imaging, perfusion-fixed globes were bisected at the equator and cleaned of vitreous, lens, and uvea. Anterior segments were then quadrisected, and the entirety of each quadrant was imaged *en face*. Quadrant images were pieced together to reconstruct the macro-scale tracer pattern around the entire circumference (Fig. 2), with orientation defined based on the arrangement of the extraocular muscles. We used a Nikon TE-2000E microscope with Coolsnap ES Monochrome camera, 10× internal magnification, 1× objective (0.04 NA), and appropriate barrier filters for macro-scale imaging of each tracer color. Images of isolated tracer spots on a glass slide were used to confirm negligible spectral overlap. Quadrants were stored at 4°C in phosphate-buffered saline with 0.1% PFA.

Micro-scale imaging was performed using confocal microscopy that was applied through tissue blocks dissected from the trabecular meshwork (LSM 510 META; Zeiss). Blocks extended 2 to 3 mm along the circumference of the limbus and were bisected along their length to expose a frontal section through the trabecular meshwork and Schlemm's canal. Tissue blocks were mounted in home-made depression slides with blue fluorescent nuclear dye (DAPI; Invitrogen) that was included within the mounting medium to provide background tissue staining. Regions of

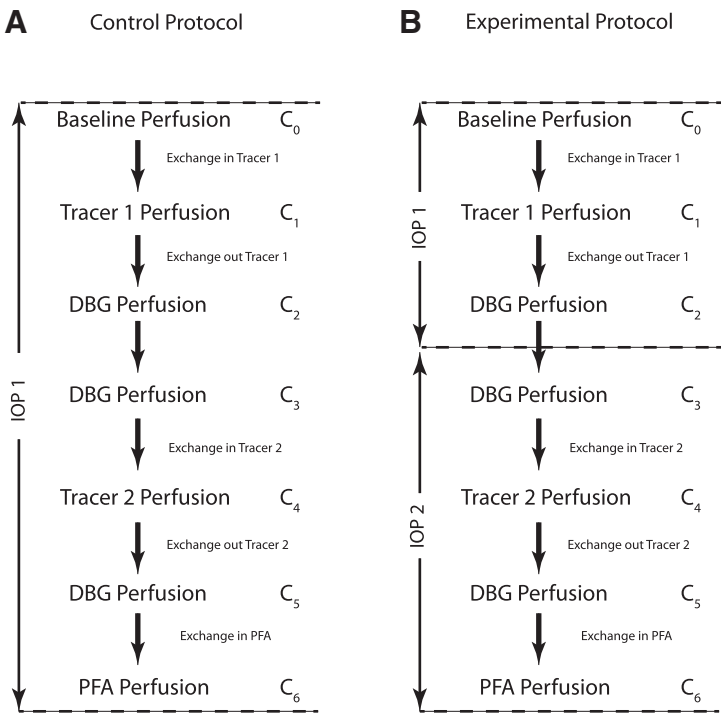

FIG. 1. Summary of the perfusion protocol for control **(A)** and experimental **(B)** eyes. Each eye was perfused with DBG to measure baseline outflow facility (C_0). The first tracer was then exchanged into the anterior chamber, and facility was measured while perfusing the first tracer in DBG (C_1). The first tracer was then exchanged out of the anterior chamber, and facility was measured while perfusing DBG without tracer (C_2). Intraocular pressure (IOP) was then changed in experimental eyes while IOP was maintained constant in control eyes, and facility was measured without tracer (C_3). The second tracer was then exchanged into the anterior chamber, and facility was measured while perfusing the second tracer (C_4) in DBG. The second tracer was then exchanged out of the anterior chamber, and facility was measured while perfusing DBG without tracer (C_5). Fixative, 4% paraformaldehyde (PFA), was then exchanged into the anterior chamber, and facility was measured while perfusing fixative (C_6).

the inner wall and JCT were chosen irrespectively of local tracer signal, and confocal z-stacks were acquired at 200×(20–40 μm top to bottom) using multi-track mode to separately acquire images of the first and second fluorescent tracer. To eliminate spectral bleed-through between the 2 tracer emissions, images were acquired for both tracers simultaneously at the corresponding peak emission wavelength while exciting near the peak excitation of only one tracer. Two-photon mode was used to image DAPI nuclear stain and tissue autofluorescence.

Tracer analysis: macro-scale

To quantify the fraction of the trabecular meshwork that was labeled with tracer, we segmented each quadrant image of trabecular meshwork into tracer-labeled and tracer-unlabeled regions, and measured the fraction of tracer-labeled pixels relative to the total number of pixels within the trabecular meshwork. To define an objective segmentation threshold for each image, we used an Otsu algorithm that calculates the pixel intensity threshold which minimizes within-class variance between tracer-labeled and tracer-unlabeled regions. This analysis was done separately for each of the 48 quadrants, and the area-weighted average over 4 quadrants was defined as the tracer-labeled fraction for the corresponding eye.

To quantify how macro-scale outflow patterns change in response to IOP within individual eyes, we used image subtraction to quantify differences between the first and second tracer patterns within individual quadrants. Images

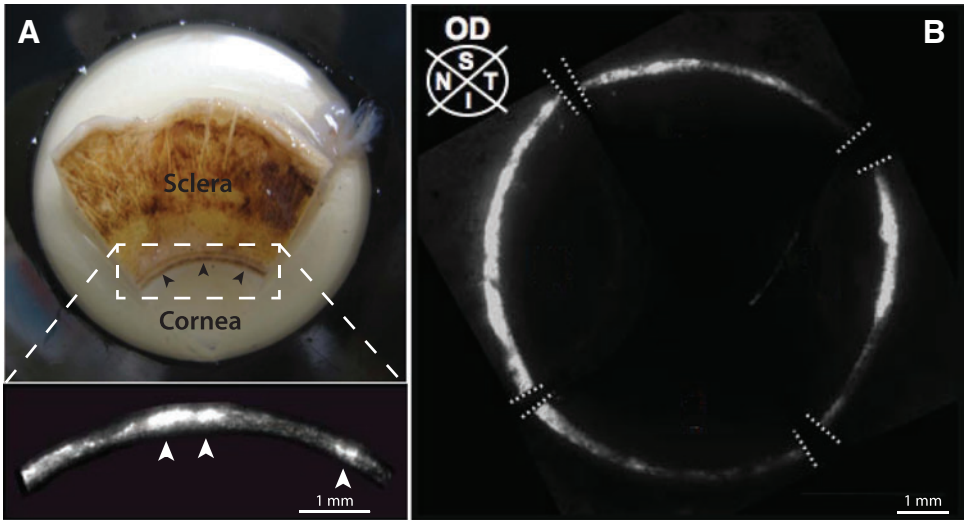

FIG. 2. **(A)** Macro-scale tracer image shown segmental filtration patterns (arrowheads) in the trabecular meshwork of an enucleated human eye perfused with fluorescent microspheres. **(B)** Four images, each containing one quadrant, were pieced together and displayed on the same intensity scale. Dotted lines indicate where quadrants were cut. S, superior; T, temporal; I, inferior; N, nasal.

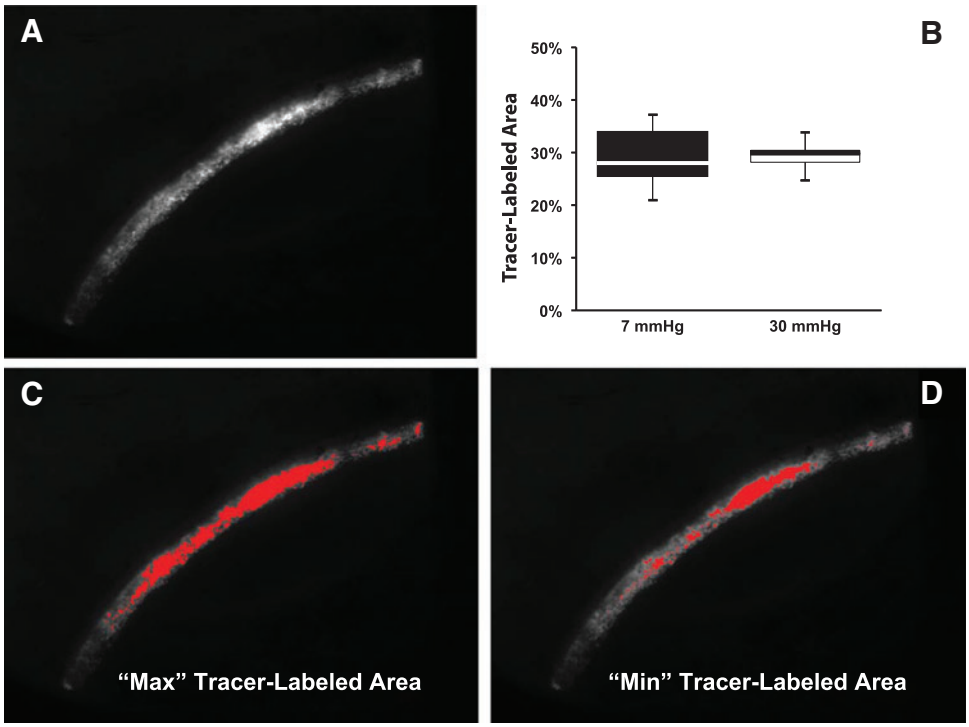

FIG. 3. Macro-scale fluorescent tracer patterns in each quadrant **(A)** were quantified and averaged (area-weighted) using an Otsu auto-threshold to measure the macro-scale tracer-labeled fraction of trabecular meshwork per eye **(B)**. Bars in the box-and-whisker plots represent the range of tracer-labeled fraction over all eyes ($N=6$ eyes per condition). Representative upper **(C)** and lower **(D)** bounding estimates of the tracer-labeled fraction (shown in red) for the quadrant shown in **(A)** as determined by 2 independent observers (S.J.F., S.N.L.).

were first background corrected by subtracting the average pixel value calculated from 3 regions of interest (ROIs) from the sclera or cornea. The resulting images were then normalized according to

$$G_i^* = \frac{G_i - \mu_G}{\sigma_G} \qquad R_i^* = \frac{R_i - \mu_R}{\sigma_R} \qquad \text{Equation 1,}$$

where G_i and R_i represent the fluorescence intensity of the first (G, green) and second (R, red) tracer, respectively, for the *ith* pixel, and the asterisks indicate the corresponding normalized values. μ_G and μ_R represent the mean pixel values for the first and second tracer across the background-corrected trabecular meshwork, while σ_G and σ_R represent the corresponding standard deviations. This normalization replaces the integer intensity value of each pixel by a real number (may be positive or negative) that represents the difference (in units of standard deviation) between the pixel intensity and the mean intensity over the meshwork region for any one quadrant. For example, a value of $+1$ (or -1) represents a pixel intensity that is one standard deviation greater (or less) than that of the mean. Importantly, this normalization preserves the tracer pattern, while adjusting for the intrinsic brightness differences between the 2 tracer colors such that the pixel intensity values become referenced to the same quantitative scale. Finally, we calculate a difference image ($D^*=R^*–G^*$) that represents the subtraction of the 2 tracer patterns in units of standard deviation. We define pixels that have a difference of greater than one standard deviation ($D^*<-1$ or $D^*>1$) as representing sites in the trabecular

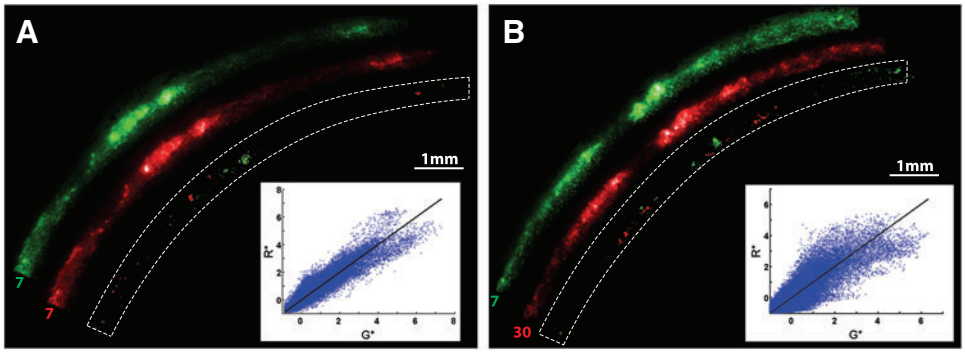

FIG. 4. Macro-scale tracer patterns exhibit subtle changes in response to changing IOP. Green and red macro-scale tracer images (normalized) from the same quadrants are displayed side by side with subtracted images shown within the dashed borders. For clarity, only pixels with a difference greater than one standard deviation are shown in the subtracted image, where the color of each pixel in the subtracted images indicates the tracer color that is more intense at that location. The images in **(A)** are taken from a control eye perfused throughout at 7 mmHg, while those in **(B)** are from the contralateral eye perfused first at 7 mmHg (green) and then at 30 mmHg (red). Insets show scatterplots of normalized red (R*) versus normalized green (G*) pixel intensities, where the data cluster about the black line representing perfect correlation (slope of unity).

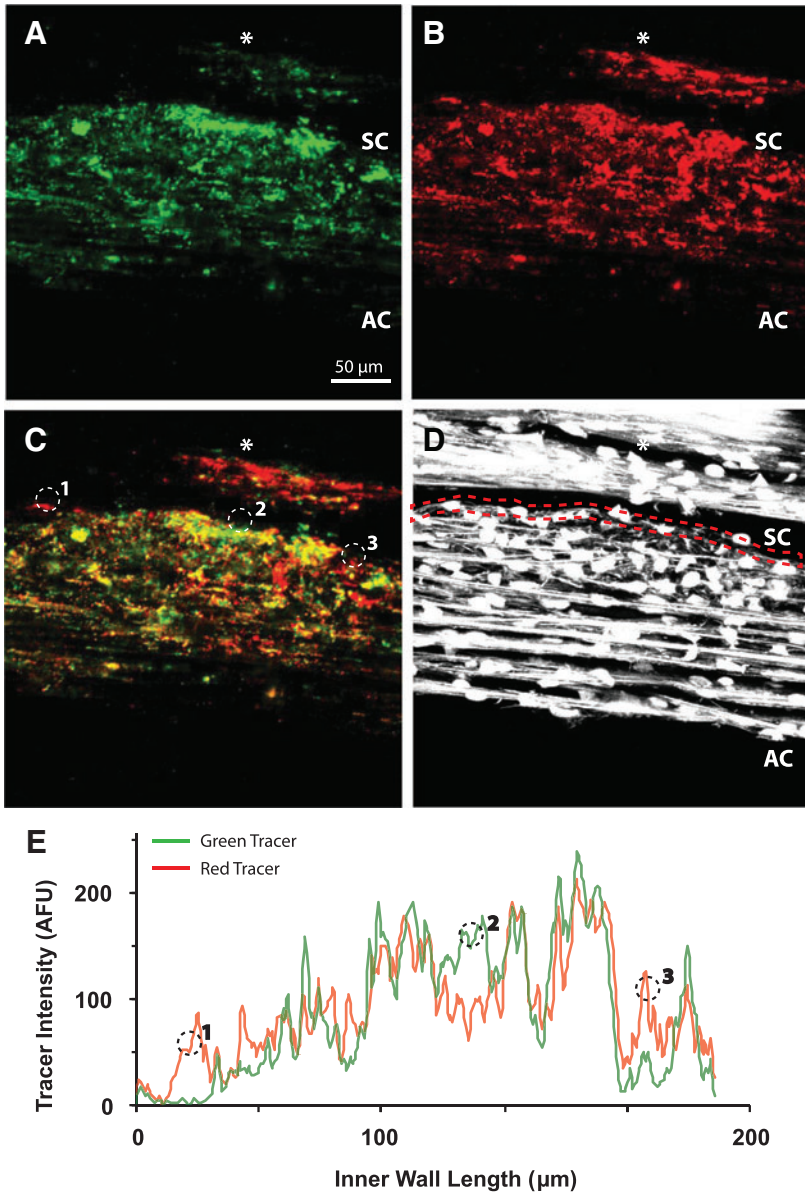

FIG. 5. Micro-scale tracer patterns through the trabecular meshwork and Schlemm's canal (SC) in an eye perfused with green tracer **(A)** at 7 mmHg, followed by red tracer **(B)** at 30 mmHg. Color-merged image shown in **(C)** shows co-localized regions in yellow. **(D)** A piece-wise linear region of interest (ROI) (red outlines, 10 µm thick) was selected along the juxtacanalicular connective tissue (JCT) and inner wall of Schlemm's canal based on tissue autofluorescence as seen by 2-photon confocal microscopy. **(E)** The fluorescence intensity profile of each tracer (averaged across the ROI thickness) plotted as a function of length along the JCT and inner wall (corresponding to the ROI shown in **(D)**). The tracer profiles were used for co-localization analysis, as described in the text. Tracer profiles were largely conserved between the 2 tracer colors, but there were small regions of differential tracer labeling indicated by the dotted numbered circles (numbers correspond to the same locations along the inner wall between **(C and E)**. Asterisks indicate the lumen of a collector channel.

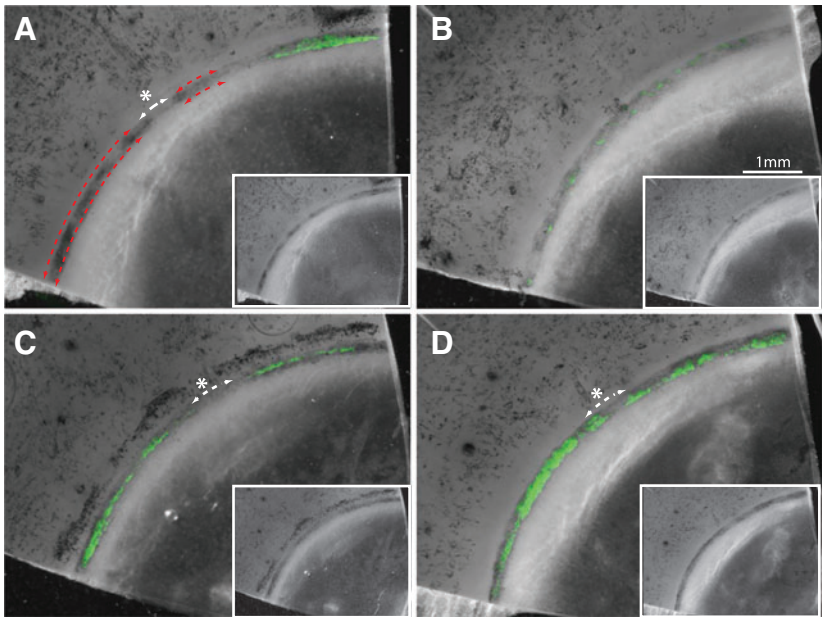

FIG. 6. Macro-scale tracer patterns do not perfectly reflect pigment distribution in the trabecular meshwork. Macro-scale tracer images (green) were registered and overlaid on brightfield images from the same quadrant **(A, B**: nasal quadrants; **C, D**: inferior quadrants, from contralateral eyes of the same individual). *Red dashed arrows* indicate regions of heavy pigmentation that appear devoid of tracer, while *white dashed arrows* (asterisks) indicate regions of low pigmentation that also appear devoid of tracer. Inset shows the same brightfield image without tracer.

TABLE 1. OUTFLOW FACILITY DATA (MEAN ± SD) USING THE FACILITY NOMENCLATURE ($C_0, C_1, \ldots$) DEFINED IN FIGURE 1

IOP_1		IOP_2	IOP_1			IOP_2			
(mmHg)			C_0	C_1	C_2	C_3	C_4	C_5	C_6
7	→	7	0.45 ± 0.22	0.39 ± 0.22	0.37 ± 0.21	0.38 ± 0.22	0.34 ± 0.20	0.33 ± 0.17	0.21 ± 0.16*
7	→	30	0.35 ± 0.21	0.36 ± 0.23	0.37 ± 0.22	0.32 ± 0.18	0.26 ± 0.16	0.25 ± 0.14	0.12 ± 0.05
30	→	30	0.32 ± 0.11	0.24 ± 0.07	0.23 ± 0.06	0.23 ± 0.08*	0.19 ± 0.03	0.18 ± 0.03	0.07 ± 0.01
30	→	7	0.36 ± 0.21	0.29 ± 0.15	0.27 ± 0.22	0.35 ± 0.32*	0.35 ± 0.22	0.39 ± 0.17	0.23 ± 0.09

$N = 3$ except where $N = 2$ as indicated by asterisks.
IOP, intraocular pressure.

meshwork where there is a significant change in macro-scale tracer patterns. Images with pixel saturation were excluded from analysis or were re-imaged at a lower exposure. This analysis was applied separately to all 48 quadrants.

Tracer analysis: micro-scale

To quantify tracer patterns at the micro scale and how these change in response to IOP, we measured the fluorescent tracer intensity along the inner wall and compared the pattern between the 2 tracer colors. An analysis was performed on the maximum intensity projection through individual confocal z-stacks (typical depth of 10–20 μm). Using the segmented line tool (ImageJ, NIH), a piecewise linear ROI was drawn along the inner wall endothelium of Schlemm's canal as visualized in the autofluorescent image. Each ROI extended approximately 230 μm along the inner wall, and the thickness of the ROI was defined to be 10 μm to include both the inner wall and JCT. The tracer intensity profile was measured along the ROI (averaged across the segmented line width) using the plot profile tool (ImageJ). This returns an array of intensity values for each tracer as a function of distance along inner wall/JCT (cf. Fig. 5E) that were used for segmentation and co-localization analysis, as described next. The same ROI was applied to both tracer colors.

To obtain an objective measure of the linear fraction of inner wall/JCT labeled with tracer, we used an automated Otsu threshold algorithm to segment tracer-labeled versus -unlabeled regions along each piecewise linear ROI. The Otsu algorithm was applied to each tracer color separately, and the tracer-labeled fraction was calculated as the ratio of labeled versus total pixels along each ROI. Any images with pixel saturation in either of the tracer channels were excluded or re-imaged. In total, 133 confocal stacks were included in this analysis from at least 2 (typically 3) quadrants from each of the 12 eyes (~11 stacks per eye).

Co-localization analysis was used to quantify the differences between the 2 tracer patterns within individual confocal stacks. To account for intrinsic brightness differences between the 2 tracer colors, the second (red) tracer in each image was scaled by a factor that minimizes the mean-squared error between the 2 tracer profiles according to

$$scaling\ factor = \frac{\sum G_i \times R_i}{\sum R_i^2} \qquad \text{Equation 2,}$$

where the summations represent the sum over all intensity values along the corresponding ROI. Importantly, this transformation preserves the tracer pattern, and enables an objective comparison between the 2 tracer profiles by accounting for intrinsic brightness differences between the tracer particles.

Statistics

Changes in outflow facility within individual eyes were analyzed using a paired 2-tailed Student's *t*-test, comparing outflow facility before and after changing IOP or tracer perfusion. Differences in macro-and micro-scale tracer patterns were analyzed using a paired 2-tailed Student's *t*-test when comparing between contralateral eyes and an unpaired 2-tailed Student's *t*-test when comparing between unpaired eyes. Linear regressions were calculated using Excel (Microsoft), with significance based on whether the slope of the linear regression was statistically different from zero, as determined by the *t*-statistic defined as the predicted slope divided by standard error of the predicted slope with *N*-2 degrees of freedom, where *N* is the total number of data points in the regression. For all cases, the significance threshold was defined to be 0.05.

Results

Outflow facility

The average baseline outflow facility (C_0) was 0.40 ± 0.20 μL/min/mmHg (mean ± SD; $N = 6$) at 7 mmHg and 0.34 ± 0.15 μL/min/mmHg ($N = 6$) at 30 mmHg. There was a nearly significant correlation between decreasing C_0 and donor age ($P = 0.09$; $N = 12$). Comparing facility before and after changing IOP within individual eyes (C_2 vs. C_3, Table 1) revealed that facility tended to increase when IOP was lowered and decrease when IOP was elevated, which was consistent with earlier reports,[19,20] but the relationship between facility and IOP did not achieve statistical significance ($P = 0.14$; paired Student's *t*-test, $N = 5$ pairs). However, perfusion with tracer microspheres at 30 mmHg coincided with a decrease in outflow facility by 24% ± 9% (C_0–C_2/C_0; $P = 0.01$, paired Student's *t*-test, $N = 6$) after perfusion with the first tracer bolus and a further decrease of 19% ± 12% (C_3–C_5/C_3; $P = 0.03$; paired Student's *t*-test, $N = 6$) after perfusion with the second tracer bolus. In contrast, there was no change in facility at 7 mmHg after perfusion with the first (6% ± 17%; $P = 0.4$, $N = 6$) or second (−11% ± 46%; $P = 0.7$; $N = 5$) tracer bolus. These data suggest that perfusion with a 100 μL bolus of tracer microspheres (0.2 μm diameter, 0.002% v/v) is sufficient to partially obstruct trabecular outflow and decrease

facility, but the magnitude of this effect is greater for larger values of IOP. It should be noted that the facility change induced by tracer is comparable to the facility changes imposed by changing IOP, such that the presence of tracer may have partly masked the relationship between facility and IOP.

Tracer patterns: macro-scale

Macro-scale imaging revealed a non-uniform or segmental distribution of tracer decoration within the human trabecular meshwork (Fig. 2). Local regions of intense decoration were observed as varying in size from focal spots that were ~100 μm wide to broad regions extending several millimeters. Tracer patterns were not conserved between paired eyes, and there was no obvious labeling pattern between quadrants that was consistent across eyes. The heterogeneous tracer distribution was not attributable to preferential sedimentation of microspheres, because changing the orientation of the eye between the first and second tracer perfusions did not affect the observed pattern.

Otsu estimates of the tracer-labeled areal fraction of trabecular meshwork for each eye ranged from 21% to 37% (mean ± SD: 29% ± 5%, $N = 12$ eyes). The tracer-labeled fraction was nearly identical between eyes perfused at 7 mmHg (29% ± 6%, $N = 6$) and eyes perfused at 30 mmHg (29% ± 4%, $N = 6$; Fig. 3). There was no significant difference in the tracer-labeled fraction between quadrants, although there was a trend for higher labeling in the nasal quadrant (26% ± 8% for inferior, 29% ± 9% for temporal, 30% ± 11% for superior, and 31% ± 13% for nasal). There was no apparent correlation between outflow facility measured during the tracer perfusion (C_1) and the tracer-labeled fraction (Supplementary Fig. S2A; $P = 0.36$), and there was no apparent correlation between tracer-labeled fraction and donor age ($P = 0.24$, $N = 12$). All analyses cited earlier were based on the first tracer only.

To validate the Otsu measurements, 2 independent observers (S.J.F., S.N.L.) each produced subjective upper and lower bounding estimates of the tracer-labeled fraction for each eye (Fig. 3C, D). Although there was significant variability in the tracer-labeled fraction between observers, the maximum observer-defined fraction never exceeded 54% for a given eye, suggesting that regardless of using an objective Otsu threshold or subjective observer threshold, no more than one-third to one-half of the trabecular meshwork appeared to be tracer labeled.

To determine whether macro-scale tracer patterns were sensitive to IOP within individual eyes, we quantitatively examined differences between the patterns of the first and second tracer (Fig. 4). Individual quadrant images were normalized and subtracted as described in the ''Methods'' section (Equation 1). The area of trabecular meshwork exhibiting a significant pattern change between the 2 tracers ($D^* > 1$ or $D^* < -1$) was larger in experimental eyes where the pressure was changed (16% ± 6%; $N = 6$) compared with control eyes where pressure was held constant (4% ± 3%; $P = 0.002$). Similarly, the Pearson's correlation coefficient between R^* and G^* was nearer to unity (representing perfect pattern co-localization between the 2 tracers) in control eyes (0.89 ± 0.05; $N = 6$) compared with experimental eyes (0.71 ± 0.11; $P = 0.002$; Fig. 4 insets). However, there was no apparent correlation between the Pearson's correlation coefficient and the change in outflow facility between the 2 tracer perfusions (C_5/C_2; $P = 0.20$). These data indicate that changing IOP introduced subtle, but statistically detectable, changes in the macro-scale distribution of tracer in the trabecular meshwork, while maintaining the same overall tracer-labeled fraction.

Tracer patterns: micro-scale

Micro-scale confocal imaging of tracer patterns revealed a non-uniform distribution of tracer labeling within the trabecular meshwork, with the highest tracer intensity in the trabecular meshwork often observed in the JCT underlying the inner wall of Schlemm's canal (Fig. 5). Two-photon imaging provided excellent tissue contrast, revealing the structure of trabecular beams, cell nuclei (DAPI), and dense sclera, with Schlemm's canal and collector channels obviously visible by the presence of a dark lumen (Fig. 5D). While it was possible to visually identify focal sites along the inner wall that appeared to have the highest tracer labeling, some amount of tracer was often observed along the entire length of the inner wall and JCT, rendering subjective assessment ambiguous.

To objectively quantify the tracer-labeled fraction along the inner wall and JCT, we selected a segmented linear ROI (10 μm thick; dotted outline in Fig. 5D) along the inner wall of each confocal stack and measured the tracer intensity profile along the ROI (Fig. 5E). As defined by an Otsu autothreshold, the tracer-labeled linear fraction along the inner wall/JCT ranged from 7% to 30% (mean ± SD: 21% ± 6%; $N = 12$ eyes), but there was significant variability (~60%) between ROIs within individual eyes. There was no significant difference ($P = 0.62$) in the tracer-labeled fraction of inner wall/JCT between eyes perfused at 7 mmHg (20% ± 7%; $N = 6$ eyes) versus eyes perfused at 30 mmHg (21% ± 5%; $N = 6$ eyes), and there was no apparent correlation with outflow facility (C_1, Supplementary Fig. S2B; $P = 0.71$) or donor age ($P = 0.58$). All the earlier analysis was based on the first tracer only.

To examine how micro-scale tracer patterns changed within individual eyes in response to changing IOP, we performed co-localization analysis between the intensity profile of the 2 tracers within each ROI (Fig. 5E). The Pearson's correlation coefficient (r) indicated that there was significant co-localization between the 2 tracers ($r = 0.56 \pm 0.14$; $N = 12$ eyes; $P = 2 \times 10^{-8}$). However, there was no apparent statistical difference in Pearson's correlation coefficient between control eyes that were perfused at the same IOP (0.63 ± 0.12) compared with experimental eyes where IOP was changed (0.49 ± 0.12; $P = 0.18$, paired Student's t-test; $N = 6$ pairs). There was also no apparent correlation between the Pearson's correlation coefficient and the C_5/C_2 ratio that represents the change in outflow facility between the first and second tracer perfusion ($P = 0.40$). Although a larger number of samples may have revealed a statistical difference between experimental and control eye (a *post-hoc* power calculation predicts that 9 pairs are required to achieve $\beta = 0.20$ and $\alpha = 0.05$ assuming the Pearson's correlation coefficients given earlier), these data suggest that micro-scale tracer patterns along the inner wall and JCT of human eyes appear relatively insensitive to changes in IOP over hour-long time scales.

Relationship between tracer, pigmentation, and collector channels

To examine the spatial relationship between tracer and pigmentation, fluorescent images of macro-scale tracer distribution were co-registered and overlapped onto bright-field images of the pigment distribution from the same quadrant (Fig. 6). In some areas, there was an apparent co-localization between tracer and pigment in the trabecular meshwork (Fig. 6C, D), but in other quadrants (even from the same eye), there were regions of relatively heavy pigmentation that were relatively devoid of tracer (Fig. 6A, B). To quantify this relationship, we performed a co-localization analysis between local tracer and pigmentation as measured by pixel intensity values. To do this, while allowing for small co-registering errors, we divided the trabecular meshwork into contiguous regions spanning 5° arcs along the trabecular meshwork circumference and bounded by the anterior and posterior margins of the trabecular meshwork, and we calculated the average pixel intensity of tracer and pigment in each region. Including images from 45 quadrants (3 quadrants could not be co-registered) yielded a modest Pearson correlation coefficient between pigment and tracer intensity ($r = 0.17 \pm 0.45$, $R^2 = 0.22 \pm 0.24$; mean ± SD) that was significantly different from zero ($P = 0.017$). This suggests that while tracer, indeed, tends to coincide with sites of heavier pigmentation, the relationship is relatively weak and cannot account for more than approximately 22% of the observed variability.

To examine the potential role of collector channels in segmental outflow,[9] we isolated tissue wedges from regions of trabecular meshwork containing high or low macro-scale tracer intensity (Fig. 7A, B). Frontal sections through the trabecular meshwork and Schlemm's canal were then examined by 2-photon microscopy to identify collector channels and collector channel ostia (Fig. 7D–F). Overall, we examined 47 wedges from 12 eyes, with 2–3 confocal stacks (20–40 μm thick) per wedge. Of 22 low-tracer wedges, only 4 (18%) were found with observable collector channels and none had observed ostia. In contrast, of 25 high-tracer wedges, 15 (60%) had observable collector channels with 10 of these (40%) having observed ostia (Fig. 7C). It is important to note that only a fraction of the total tissue volume was sampled from each wedge, which almost certainly underestimates the presence of collector channels. However, a similar tissue volume was examined in both high and low tracer-labeled wedges. Therefore, despite the relatively small sample size and limited penetration of confocal imaging, the difference in the observed numbers of collector channels between high and low tracer-labeled wedges suggests that regions of high macro-scale tracer labeling tend to coincide with collector channel ostia, which was consistent with a previous report.[9]

Discussion

This study examined segmental outflow patterns in the trabecular meshwork of enucleated human eyes, as visualized by perfusion with fluorescent tracer microspheres, and investigated whether segmental outflow patterns were sensitive to IOP and outflow facility. The experimental design incorporated a 2-color tracer strategy previously described

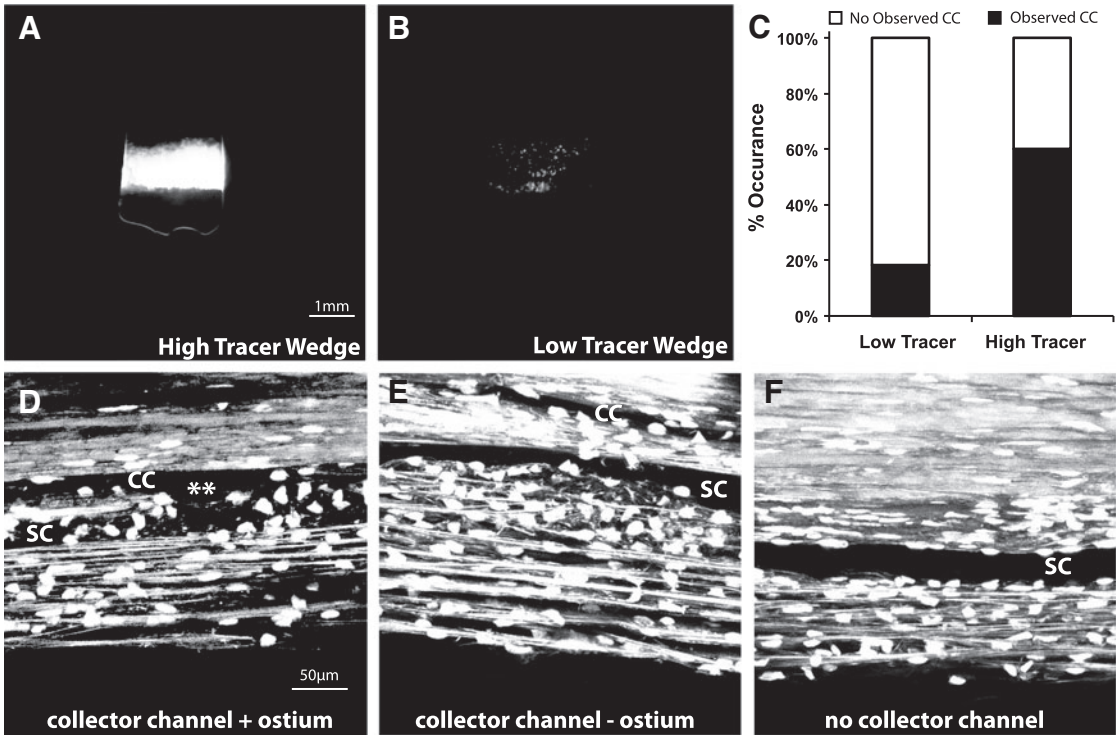

FIG. 7. The relationship between macro-scale tracer intensity and collector channels was examined in high **(A)** and low **(B)** tracer-labeled tissue wedges using 2-photon confocal microscopy. The presence of collector channels with an observed ostium (asterisks) **(D)**, collector channels without an observed ostium **(E),** and the apparent absence of any collector channel **(F)** were assessed in 47 macro-scale tissue wedges. **(C)** The relative occurrence of collector channels (with or without ostia) was 3-fold larger in high tracer- compared with low tracer-labeled wedges.

for bovine eyes[13,14], where green tracer was perfused at baseline pressure followed by red tracer after changing IOP. This experimental design is advantageous, because pre- and post-stimulus tracer patterns can be directly compared within individual sections, thereby increasing the statistical power to detect subtle pattern changes despite significant regional heterogeneity in segmental tracer distribution. Tracer patterns were examined over macro-scale (0.1–10 mm) and micro-scale (10–100 μm) dimensions. Overall, we observed relatively modest, yet statistically detectable, changes in macro-scale tracer patterns in response to changing IOP, and we observed no significant differences in micro-scale tracer patterns in response to changing IOP. There was also no apparent correlation between outflow facility and macro- or micro-scale tracer-labeled fractions. These data suggest that segmental outflow patterns in enucleated human eyes are relatively insensitive to outflow facility and changing IOP between 7 and 30 mmHg over hour-long time scales.

There are 2 fundamental assumptions underlying this study (and all tracer studies for that matter): (1) that tracer labeling patterns represent sites of active filtration in the trabecular meshwork; and (2) that tracer patterns observed in enucleated human eyes are representative of aqueous humor filtration patterns as would occur *in vivo*. The validity of these assumptions is difficult to confirm. However, we point to the precedent set by a number of prior studies in human,[9,17,21] monkey,[16,22] bovine,[7,8,13–15] porcine,[21] and murine[23] eyes that used similar fluorescent tracers to study aspects of segmental outflow. No studies have directly compared segmental outflow patterns between living and enucleated human eyes, but there is evidence based on pigment distribution that outflow segmentation occurs in living humans.[9–12]

Perhaps the most intriguing finding of this study was the observation that only about one-third ($29\% \pm 5\%$) of the macro-scale trabecular meshwork is tracer labeled, with a somewhat smaller fraction ($21\% \pm 6\%$) of micro-scale tracer labeling along the inner wall of Schlemm's canal and JCT. If these values are representative of filtration patterns as occur in living human eyes, then segmental outflow becomes an important consideration in the design and delivery of anti-glaucoma therapies that are aimed at improving conventional outflow. That is because any molecular therapeutic will likely be distributed preferentially to sites of active filtration in the trabecular meshwork, with less effective diffusion-limited delivery to non-filtering regions. Since it is the non-filtering portions of trabecular meshwork that most likely contribute to outflow obstruction in glaucoma, strategies which target non-filtering tissues may need to be developed to realize the full potential of outflow-enhancing drugs, particularly for glaucomatous eyes where the active filtration area appears even further reduced.[5] It is useful to point out that rho-kinase inhibitors (RKIs) appear to increase the effective filtration length (EFL) along the inner wall,[8,17] suggesting that in addition to a direct effect on outflow facility, RKIs may be useful as a combination therapy to promote drug delivery to non-filtering and presumably obstructed regions of the trabecular meshwork.

A second important implication is with regard to the placement of outflow shunts and lasered sites during trabeculoplasty. Since filtration-active regions represent functional zones of the trabecular meshwork, understanding the distribution of segmental outflow may inform the surgical placement of shunts or lasered sites to achieve better overall outflow function and IOP reduction. For example, one potential strategy is to preserve filtration-active ''functional'' regions by confining shunts or lasered sites to non-filtering ''nonfunctional'' regions. This would require mapping of segmental outflow patterns in living patients, which may be possible based on pigment distribution as seen by gonioscopy (see discussion on pigmentation below) or with ongoing advancements in anterior segment optical coherence tomography.[24]

Despite changing IOP between 7 and 30 mmHg, we observed only modest changes in the macro-scale tracer patterns and no apparent changes in the micro-scale patterns, and there was strong co-localization between the 2 tracer colors within individual eyes. Furthermore, we did not observe a statistically significant correlation between outflow facility and the extent of tracer labeling, or any relationships involving changes in these metrics, at either scale. These data suggest that segmental outflow patterns in human trabecular meshwork are relatively insensitive to changes in IOP and outflow facility and that tracer patterns are largely reproducible over 2–3 h of perfusion without significant tracer loss from the trabecular meshwork. These results, however, are inconsistent with a number of prior reports[7,8,13–16] describing a significant correlation between outflow facility and EFL that is analogous to the micro-scale tracer-labeled fraction along the inner wall and JCT. The reasons for this inconsistency remain unclear. However, most prior studies that examined the effect of IOP elevation on tracer patterns were done in bovine eyes,[7,13,14] and there may be species-dependent differences in the mechanical compliance[25] or anatomy of the trabecular meshwork (discontinuous aqueous plexus in bovine versus continuous Schlemm's canal in humans) that influence the relationship between tracer patterns and facility. The tracer studies that were published to date in humans examined the effect of an RKI (Y-27632),[17] and it is possible that the mechanisms of facility increase caused by an RKI (eg, changes in the hydraulic conductivity of the inner wall or JCT) differ from the mechanisms of facility increase caused by changing IOP (eg, dimensional changes in Schlemm's canal[26]). There also may have been differences in acquisition of the tracer images, particularly with regard to image saturation, and how the tracer patterns were quantified between studies (eg, objective versus subjective metrics). Regardless, understanding the basis for the different IOP and facility responses between studies and between human and nonhuman eyes may improve our understanding of the factors controlling segmental outflow in the trabecular meshwork.

The factors controlling segmental outflow are likely important determinants of outflow function and IOP regulation. Prior studies have shown that tracer labeling patterns in the trabecular meshwork coincide with the distribution of extracellular matrix (ECM) proteins, such as versican[21] and SPARC,[23] suggesting that accumulation of ECM proteins may influence local hydraulic conductivity through the trabecular meshwork. Morphological correlates of segmental outflow have also been described in bovine,[15] monkey,[16] and human[9,17] eyes where regions of greater tracer labeling coincide with local separation between the endothelial lining of Schlemm's canal and the underlying JCT, which has been described as disrupting the ''funneling'' effect[27] and leads to a local increase in hydraulic conductivity.[18] Our study found that macro-scale tracer patterns tend to coincide with the

distribution of collector channel ostia, consistent with prior reports.[7,9] Taken together, these data are consistent with a multi-scale hypothesis governing segmental outflow in the trabecular meshwork, where macro-scale regions of filtration are influenced by the distribution of collector channel ostia and micro-scale regions of filtration are influenced by local ECM accumulation and the morphology of the inner wall of Schlemm's canal. In partial support of this multi-scale hypothesis, we point out that micro-scale regions of inner wall and JCT were not uniformly labeled, even in macro-scale regions that had the highest apparent tracer labeling intensity. It remains to be determined how macro- and micro-scale outflow segmentation are coupled, whether these patterns are static or dynamic, and whether one particular length scale has a dominant role in outflow resistance regulation. Important additional considerations are the possible non-uniform distribution of episcleral venous pressure[28] and, for enucleated eyes, the role of perfusate retention within the conjunctiva and Tenon's capsule[24] that may influence downstream pressure conditions to affect segmental outflow or tracer-labeling patterns.

Prior studies have suggested that trabecular pigmentation may serve as an endogenous marker of outflow segmentation[10–12] and that pigment and tracer patterns overlap in perfused human eyes.[9] Our study examined the co-localization between pigment and macro-scale tracer patterns over nearly the full circumference of 12 eyes. While we found that regions of greater tracer intensity, indeed, tend to coincide with regions of heavier pigmentation, we often observed regions of heavy pigmentation that were relatively devoid of tracer (Fig. 6). It is important to note that our studies similar to others[9] were done using *ex vivo* enucleated eyes, and, therefore, any colocalization between pigmentation and outflow patterns that may have existed *in vivo* could have been disturbed by postmortem changes or by conditions associated with enucleated eye perfusion (eg, changes in the distribution of episcleral venous pressure). However, if *ex vivo* tracer patterns were reflective of trabecular outflow patterns as occurred *in vivo*, then the weak correlation between tracer and pigment would suggest that pigmentation may serve only as a partial indicator, but not a substitute, for segmental outflow. It may be possible, however, that heavy pigmentation could have obscured local tracer fluorescence such that heavily pigmented regions only appear devoid of tracer, or it may be possible that regions of heaviest pigmentation represent sites which have become obstructed by excessive pigment deposition. Alternatively, pigment may have been deposited over months to years, while segmental outflow patterns may change over shorter time scales, such that some pigmented regions may represent temporality inactive regions of trabecular outflow. Regardless, more research is needed to further examine the relationship between pigmentation and segmental outflow in living eyes, as this may offer the advantage of mapping segmental outflow in patients based on pigmentation distribution as seen using gonioscopy.

The opportunity to label filtration-active regions using fluorescent tracers offers the potential to improve morphometric and biochemical assessments of the factors controlling outflow resistance generation within the trabecular meshwork. Since only approximately one-third of human trabecular meshwork appears to be filtration-active, studies using indiscriminate microscopy sections or excised tissue from the trabecular meshwork would likely comprise a larger contribution from non-filtering regions. In contrast, studies that discriminate active from inactive filtration regions (as identified by high versus low tracer intensity after perfusion) may reveal new insights into the mechanisms controlling segmental outflow and resistance generation within the trabecular meshwork. We point out that recent studies have successfully exploited this technique to demonstrate the potential role of versican in outflow segmentation.[21]

In conclusion, this study examined tracer-labeling patterns in the trabecular meshwork of enucleated human eyes as a marker of segmental outflow occurring over macro-scale and micro-scale dimensions. Only approximately one-third of human trabecular meshwork appears to be filtration-active, and tracer-labeling patterns appear to be relatively insensitive to outflow facility and changes in IOP over hour-long time scales. There is a modest co-localization between tracer and pigment distribution, and regions of high macro-scale tracer labeling tend to coincide with the presence of collector channel ostia. Segmental outflow is likely important for drug delivery to the trabecular meshwork by limiting delivery to non-filtering or obstructed regions, and designs that improve drug delivery to non-filtering regions may better realize the improvement of overall trabecular outflow function.

Acknowledgments

The authors acknowledge the contribution of Stephanie M. Roberts, B.S., who contributed to the development of the quantitative tracer algorithms. They acknowledge the support of donors to National Glaucoma Research, a program of the American Health Assistance Foundation. This work was supported by a grant (NGR-G2006-057) from the BrightFocus Foundation (formerly the American Health Assistance Foundation).

Author Disclosure Statement

No competing financial interests exist.

References

1. Grant, W.M. Further studies on facility of flow through the trabecular meshwork. *AMA Arch. Ophthalmol*. 60(4 Part 1):523–533, 1958.
2. Grant, W.M. Experimental aqueous perfusion in enucleated human eyes. *Arch. Ophthalmol*. 69:783–801, 1963.
3. Mäepea, O., and Bill, A. The pressures in the episcleral veins, Schlemm's canal and the trabecular meshwork in monkeys: effects of changes in intraocular pressure. *Exp. Eye Res*. 49:645–663, 1989.
4. Mäepea, O., and Bill, A. Pressures in the juxtacanalicular tissue and Schlemm's canal in monkeys. *Exp. Eye Res*. 54:879–883, 1992.
5. De Kater, A.W., Melamed, S., and Epstein, D.L. Patterns of aqueous humor outflow in glaucomatous and non-glaucomatous human eyes. A tracer study using cationized ferritin. *Arch. Ophthalmol*. 107:572–576, 1989.
6. Ethier, C.R., and Chan DWH. Cationic ferritin changes outflow facility in human eyes whereas anionic ferritin does not. *Invest. Ophthalmol. Vis. Sci*. 42:1795–1802, 2001.
7. Battista, S.A., Lu, Z., Hofmann, S., Freddo, T., Overby, D.R., and Gong, H. Reduction of the available area for aqueous

humor outflow and increase in meshwork herniations into collector channels following acute IOP elevation in bovine eyes. *Invest. Ophthalmol. Vis. Sci*. 49:5346–5352, 2008.
8. Lu, Z., Overby, D.R., Scott, P.A., Freddo, T.F., and Gong, H. The mechanism of increasing outflow facility by rho-kinase inhibition with Y-27632 in bovine eyes. *Exp. Eye Res*. 86:271–281, 2008.
9. Hann, C.R., and Fautsch, M.P. Preferential fluid flow in the human trabecular meshwork near collector channels. *Invest. Ophthalmol. Vis. Sci*. 50:1692–1697, 2009.
10. Gottanka, J., Johnson, D.H., Martus, P., and Lütjen-Drecoll, E. Beta-adrenergic blocker therapy and the trabecular meshwork. *Graefes Arch. Clin. Exp. Ophthalmol*. 239:138–144, 2001.
11. Gottanka, J., Flügel-Koch, C., Martus, P., Johnson, D.H., and Lütjen-Drecoll, E. Correlation of pseudoexfoliative material and optic nerve damage in pseudoexfoliation syndrome. *Invest. Ophthalmol. Vis. Sci*. 38:2435–2446, 1997.
12. Johnson, D.H. Does pigmentation affect the trabecular meshwork? *Arch. Ophthalmol*. 107:250–254, 1989.
13. Zhu, J., Wen, Y.E., and Gong, H. Development of a novel two color tracer perfusion technique for the hydrodynamic study of aqueous outflow in bovine eyes. *Chin. Med. J*. 123:599, 2010.
14. Zhu, J.-Y., Ye, W., Wang, T., and Gong, H.-Y. Reversible changes in aqueous outflow facility, hydrodynamics, and morphology following acute intraocular pressure variation in bovine eyes. *Chin. Med. J*. 126:1451–1457, 2013.
15. Scott, P.A., Lu, Z., Liu, Y., and Gong, H. Relationships between increased aqueous outflow facility during washout with the changes in hydrodynamic pattern and morphology in bovine aqueous outflow pathways. *Exp. Eye Res*. 89:942–949, 2009.
16. Lu, Z., Zhang, Y., Freddo, T.F., and Gong, H. Similar hydrodynamic and morphological changes in the aqueous humor outflow pathway after washout and Y27632 treatment in monkey eyes. *Exp. Eye Res*. 93:397–404, 2011.
17. Yang C-YC, Liu, Y., Lu, Z., Ren, R., and Gong, H. Effects of Y27632 on Aqueous humor outflow facility with changes in hydrodynamic pattern and morphology in human eyes. *Invest. Ophthalmol. Vis. Sci*. 54:5859–5870, 2013.
18. Overby, D., Gong, H., Qiu, G., Freddo, T.F., and Johnson, M. The mechanism of increasing outflow facility during washout in the bovine eye. *Invest. Ophthalmol. Vis. Sci*. 43:3455–3464, 2002.
19. Brubaker, R.F. The effect of intraocular pressure on conventional outflow resistance in the enucleated human eye. *Invest. Ophthalmol. Vis. Sci*. 14:286–292, 1975.
20. Moses, R.A. The effect of intraocular pressure on resistance to outflow. *Surv. Ophthalmol*. 22:88–100, 1977.
21. Keller, K.E., Bradley, J.M., Vranka, J.A., and Acott, T.S. Segmental versican expression in the trabecular meshwork and involvement in outflow facility. *Invest. Ophthalmol. Vis. Sci*. 52:5049–5057, 2011.
22. Zhang, Y., Toris, C.B., Liu, Y., Ye, W., and Gong, H. Morphological and hydrodynamic correlates in monkey eyes with laser induced glaucoma. *Exp. Eye Res*. 89:748–756, 2009.
23. Swaminathan, S.S., Oh, D.J., Kang, M.H., et al. Secreted Protein Acidic and Rich in Cysteine (SPARC)-Null Mice Exhibit More Uniform Outflow. *Invest. Ophthalmol. Vis. Sci*. 54:2035–2047, 2013.
24. Kagemann, L., Wollstein, G., Ishikawa, H., et al. 3D visualization of aqueous humor outflow structures *in-situ* in humans. *Exp. Eye Res*. 93:308–315, 2011.
25. Camras, L.J., Stamer, W.D., Epstein, D., Gonzalez, P., and Yuan, F. Differential effects of trabecular meshwork stiffness on outflow facility in normal human and porcine eyes. *Invest. Ophthalmol. Vis. Sci*. 53:5242–5250, 2012.
26. Van Buskirk, E.M. Anatomic correlates of changing aqueous outflow facility in excised human eyes. *Invest. Ophthalmol. Vis. Sci*. 22:625–632, 2005.
27. Johnson, M., Shapiro, A., Ethier, C.R., and Kamm, R.D. Modulation of outflow resistance by the pores of the inner wall endothelium. *Invest. Ophthalmol. Vis. Sci*. 33:1670–1675, 1992.
28. Sit, A.J., and McLaren, J.W. Measurement of episcleral venous pressure. *Exp. Eye Res*. 93:291–298, 2011.

Received: September 1, 2013
Accepted: November 30, 2013

Address correspondence to:
Dr. Darryl R. Overby
Department of Bioengineering
Imperial College London
South Kensington Campus
Bessemer 3.07
London SW7 2AZ
United Kingdom

E-mail: d.overby@imperial.ac.uk